nature communications

Article

https://doi.org/10.1038/s41467-026-74992-z

The quantitative contribution of different Photosystem II compartments to non-photochemical quenching in *Arabidopsis*

Received: 24 February 2021

Accepted: 19 June 2026

Published online: 27 June 2026

Check for updates

Lauren Nicol[1,5], Anna Calabritto[1,5], Haidan Yao[1], Vincenzo Mascoli[1], Luca Dall'Osto[2], Roberto Bassi[2], Herbert van Amerongen[3,4] & Roberta Croce[1]

Excess excitation energy in the light-harvesting antenna of Photosystem II (PSII) can cause irreversible damage to the photosynthetic apparatus. In periods of high light intensity, a feedback mechanism known as non-photochemical quenching (NPQ) induces the formation of quenchers, which can safely dissipate excess excitation energy as heat. Although quenchers have been identified in more than one compartment of the PSII supercomplex, there is currently no quantitative description of the extent to which NPQ occurs at each of these locations. Here, we perform time-resolved fluorescence measurements on *Arabidopsis thaliana* WT and antenna mutants lacking LHCII trimers (koLHCII) and all peripheral antenna (Ch1lhcb5). By combining the results with those from steady-state fluorescence experiments, we are able to estimate the intrinsic rate of NPQ for each plant and each PSII compartment. It is concluded that more than 70% of quenching occurs in LHCII, less than 10% in the minor antenna, and the rest is associated with the PSII core.

Photosystem II (PSII) is the light-driven enzyme catalyzing the initial reactions of oxygenic photosynthesis—oxidation of water and reduction of plastoquinone (Q_A). In the thylakoid membranes of plants, PSII is surrounded by an antenna of light-harvesting complexes (LHCs), which are densely packed with chlorophylls (Chls) and carotenoids. The pigment-protein matrix facilitates both efficient light absorption and excitation energy transfer to the reaction center (RC), where photochemistry takes place.

Upon absorption of a photon and promotion of a Chl to the excited state, photochemistry can occur within 100–400 ps if the PSII RC is open (i.e. Q_A is oxidized)[1]. This is fast enough to largely outcompete excited-state decay pathways of fluorescence, internal conversion and intersystem crossing, resulting in a photochemical quantum yield of ~0.8–0.9. If the PSII RC is closed (i.e. Q_A is reduced), the Chl *a* excited-state lifetime increases to ~2 ns[2,3], increasing the probability of triplet formation. This situation can occur in high light intensities, when photon absorption exceeds the capacity of the electron transport chain. Chl triplets can then react with molecular oxygen to produce reactive oxygen species, which damage the photosynthetic apparatus and cause rapid photoinhibition[4,5].

To prevent this outcome, a feedback mechanism induces the formation of quenchers, providing an alternative excited-state decay pathway that safely dissipates the excess excitation energy as heat. This process is known as non-photochemical quenching (NPQ, for recent reviews see refs. 6–9) and in vascular plants it is triggered by an increase in lumen proton concentration[10] and subsequent protonation of the integral membrane protein PsbS[11,12]. Low pH in the lumen also activates violaxanthin de-epoxidase, which converts violaxanthin to zeaxanthin[13,14]. What happens next is largely unknown, but PsbS and zeaxanthin are thought to induce quenching sites in components of the PSII supercomplex either directly or indirectly[6,8,15].

The dimeric PSII supercomplex can be broadly split into three compartments: PSII core, minor antenna and LHCII[16,17]. The PSII core is a multi-subunit complex containing the RC and an inner antenna

[1]Biophysics of Photosynthesis, Department of Physics and Astronomy, Faculty of Science, Vrije Universiteit Amsterdam, Amsterdam, The Netherlands. [2]Laboratory of Photosynthesis and Bioenergy, Department of Biotechnology, University of Verona, Verona, Italy. [3]Laboratory of Biophysics, Wageningen University & Research, Wageningen, The Netherlands. [4]MicroSpectroscopy Research Facility, Wageningen University and Research, Wageningen, The Netherlands. [5]These authors contributed equally: Lauren Nicol, Anna Calabritto. e-mail: r.croce@vu.nl

system coordinating 35 Chls *a* per monomer. The minor antenna consists of three monomeric LHCs, Lhcb4, Lhcb5 and Lhcb6 per PSII core monomer. Together, they coordinate 38 Chls and play an important role in structurally and energetically connecting LHCII to the core[1,18]. LHCII is a trimeric complex comprised of varying combinations of the three isoforms Lhcb1, Lhcb2, and Lhcb3[19]. Depending on light conditions, there can be 1–4 trimers per monomeric core, together coordinating up to 168 Chls[20,21].

Quenching mechanisms have been proposed for each of these three compartments of the PSII supercomplex. Quenching in LHCII is largely thought to occur via a conformational change of the complex, triggered by PsbS that becomes protonated at low pH values in the lumen. This quenching is amplified by zeaxanthin (Zx), which is formed from violaxanthin (Vx) also at low luminal pH[6,15,22]. In the quenched state, a large part of the excitation energy is supposedly transferred from Chls to carotenoids, which quickly dissipate it (see[6] and references therein). An independent quenching site has also been proposed to be present in the minor antenna[23,24]. The formation of a carotenoid cation radical observed in isolated minor antenna was suggested to be responsible for the quenching in these complexes[25]. However, recent results have shown that Chl to carotenoid excitation-energy transfer can also lead to quenching in Lhcb4, suggesting that the quenching mechanism is the same in all LHCs[26,27]. Quenching in the PSII core has also been proposed, although determining the exact mechanism requires further investigation[24,28–30].

For the most part, the various quenching mechanisms have been studied in vitro, and there are questions surrounding their physiological relevance or the extent to which they contribute to NPQ in vivo. Knockout mutants lacking entire PSII compartments, therefore, represent a valuable tool in answering these questions, and the construction of a mutant lacking all minor antenna (NoM) was an important step in this regard[24]. The mutant had WT levels of NPQ, although altered induction kinetics, leading to the proposal of a multi-site model in which quenching in minor antenna and LHCII operate on different timescales. However, due to the poor energetic connection of LHCII to the core, it was difficult to determine whether the changes in NPQ were due to a loss of quenching sites or other factors[31]. Lately, Saccon et al.[32] used the same mutant, treated with lincomycin to reduce the amount of PSII core, to conclude that the capacity to switch between a light harvesting and quenching state is intrinsic to LHCII.

Generating a complete knockout of LHCII has proven more challenging, as this complex consists of 3 subunits encoded by 9 genes in *Arabidopsis thaliana* (*Arabidopsis*). A mutant lacking Lhcb1, Lhcb2, and therefore all LHCII trimers, displayed a ~60% reduction in NPQ, indicating that LHCII trimers are the dominant site of quenching[33]. However, this mutant still contains Lhcb3, which accounts for a relatively small portion (~10%) of LHCII under normal growth conditions[34,35]. More recently, a mutant lacking all three LHCII subunits has been reported[36], confirming the strong reduction of NPQ in the absence of LHCII trimers, while showing that a residual level of NPQ remains detectable even in the absence of Lhcb3.

Different strategies have been used to eliminate PSII antenna complexes entirely. The chlorina mutant (Ch1), which lacks chlorophyllide *a* oxygenase (CAO), cannot synthesize Chl *b* and therefore cannot stably accumulate functional Lhcb proteins. This mutant exhibits NPQ levels similar to those of the Lhcb1 and Lhcb2 knockout, suggesting the presence of a secondary quenching site in the PSII core[33]. However, Lhcb5 accumulated to a significant amount in this mutant, albeit likely as an apoprotein, not binding any pigments[30]. A second chlorina mutant lacking Lhcb5 (Ch1-Lhcb5) showed a further reduction in NPQ[36], limiting also the possibility of pleiotropic effects due to the presence of a misfolded antenna in the membrane.

Despite these advances, previous studies have not quantitatively resolved the contribution of each quenching site to NPQ. NPQ is typically measured via the quenching of steady-state fluorescence using pulse-amplitude-modulated (PAM) fluorometry. The value of NPQ in this instance is presumably the ratio of the rate of NPQ and the decay rate in the absence of NPQ and PSII photochemistry. However, this is only correct if there are no disconnected and unquenched antenna complexes. A direct comparison of the NPQ value between WT and antenna mutants is problematic for two additional reasons. First, the rate of NPQ is influenced by antenna size and second, it assumes the decay rate in the absence of NPQ and PSII photochemistry is the same in all plants. The substantial difference in Fv/Fm observed between mutants and WT[36] indicates that some of these assumptions do not hold.

In order to make a quantitative comparison between plants, it is necessary to directly compare the intrinsic rate of NPQ, i.e. the rate at which excitation energy decays when it is located on the Chl that is being quenched (the quenching site). In this study, we combined steady-state and time-resolved fluorescence measurements on WT and two antenna mutants. Specifically, we analyzed the koLHCII mutant, which lacks all three LHCII isoforms, and the Chl-Lhcb5 mutant that also lacks the minor antennae. This approach allows us to quantitatively assign NPQ contributions to distinct compartments of the PSII supercomplex.

Results

Steady-state fluorescence

The steady-state fluorescence intensity of a leaf is proportional to the fluorescence quantum yield and strongly depends on the rates of the other Chl excited-state decay pathways[37]. The minimal fluorescence of a dark-adapted leaf F_o corresponds to the "open state" of PSII reaction centres, where Q_A is maximally oxidized. In this scenario, almost all of the absorbed energy is used in photochemistry; hence, the yield of fluorescence is small (Fig. 1a). The maximal fluorescence of a dark-adapted leaf, F_m, corresponds to the "closed state" of PSII RC, where Q_A is maximally reduced. Here, photochemistry is blocked; therefore, the yield of fluorescence increases (Fig. 1a). The maximal fluorescence of the light-adapted leaf F_m' also corresponds to the closed state of PSII RC, but here NPQ opens up an additional non-radiative pathway for Chl excited state decay, and the yield of fluorescence decreases (Fig. 1b).

The NPQ value is calculated as the ratio between the difference of maximal fluorescence in the absence and presence of NPQ, and the maximal fluorescence in the presence of NPQ, i.e. $(F_m - F_m')/F_m'$. Only the fast and reversible component of NPQ, called qE, is considered (see Table 1). As shown in Fig. 1c and Table 1, all antenna mutants display a substantial reduction in NPQ compared to WT. A reduction in the NPQ value is often assumed to originate from a larger value of F_m', due to a smaller rate of quenching; however, it could equally result from a reduction in F_m, due to static quenching, i.e. pre-existing quenching that does not require ΔpH for induction. The value of F_v/F_m, where $F_v = F_m - F_o$, is commonly used as an indicator of PSII quantum yield, and this value is also significantly reduced in all antenna mutants (Table 1). Likewise, this could indicate a decrease in F_m and/or an increase in F_o, due to a disruption in the energetic connectivity of the PSII supercomplex.

It is not possible to discriminate between these possibilities using steady-state fluorescence, as the fluorescence intensity also depends on sample-specific parameters such as leaf area and Chl concentration. Instead, we perform time-resolved fluorescence measurements on samples in the various photosynthetic states. Here, average fluorescence lifetimes are directly proportional to fluorescence yield and independent of the above-mentioned sample properties.

Time-resolved fluorescence

Time-resolved fluorescence was used to determine both the excited-state lifetimes in the open and closed state (τ_o and τ_m, respectively) of WT and antenna mutants (Fig. 2). Average fluorescence lifetimes are directly proportional to fluorescence yields, and therefore provide

https://doi.org/10.1038/s41467-026-74992-z

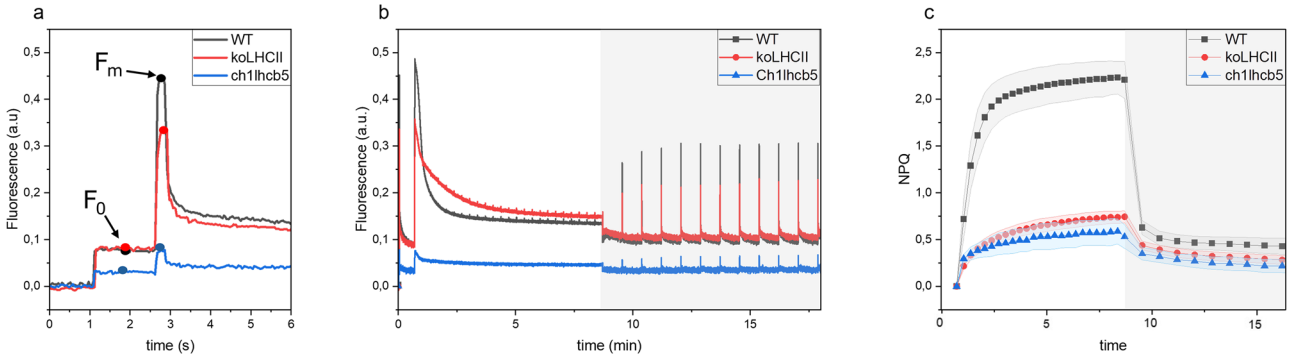

Fig. 1 | Steady-state fluorescence measurements of WT and antenna mutant leaves using PAM-fluorometry. a Raw fluorescence traces of dark-adapted leaves showing minimum chlorophyll fluorescence in the open state (F_o) and maximum fluorescence in the closed state (F_m). **b** Raw fluorescence traces of chlorophyll fluorescence quenching upon illumination with 1200 µmol photons m^{-2} s^{-1} for 8 min and chlorophyll fluorescence recovery in 10 minutes of darkness (gray background). F_m and examples of the maximum fluorescence in the light-adapted, closed state (F_m') are indicated. **c** Raw fluorescence converted to NPQ values. Data are mean ± s.d. (n = 6, 6, 4 biological replicas for WT, koLHCII, and Ch1lhcb5, respectively).

Table 1 | PAM parameters and pigment properties of WT and antenna mutants

	F_v/F_m	NPQ [a,b]	Chl *a*/*b* [c]	Chl/car [c]
WT	0.84 ± 0.01	1.79 ± 0.21	3.31 ± 0.06	3.84 ± 0.14
koLHCII	0.74 ± 0.01	0.49 ± 0.06	4.95 ± 0.05	4.13 ± 0.14
Ch1Lhcb5	0.61 ± 0.04	0.41 ± 0.09	no Chl *b*	3.10 ± 0.32

[a]Fv/Fm and NPQ data are mean ± s.d. (n = 6, 6, and 4 biological replicas for WT, koLHCII, and Ch1lhcb5, respectively).
[b]NPQ values are reported as the difference in maximum level of NPQ in light and minimum level of NPQ following dark recovery, which corresponds to the fast and reversible NPQ component, also referred to as qE (*12*).
[c]Pigment data are mean ± s.d. (n ≥ 3 biological replicas).

"absolute" values of F_o and F_m. An excitation wavelength of 468 nm was used to excite Chl *b* and carotenoids, both pigments quickly transferring excitation energy to Chl *a*[1]. Fluorescence emission was detected at 680, 700 and 720 nm with the relative emission of PSI, which has a shorter average lifetime (<100 ps)[38] in comparison to PSII, increasing in the red. To obtain more quantitative information from the decay curves, they were globally analyzed and fitted to a sum of exponential decay components (Supplementary Table 1).

Open-state measurements were performed on stacked thylakoid membranes. PSII was kept open throughout the measurement with low-power excitation and vigorous stirring of a large sample volume (Supplementary Fig. 1). The average fluorescence lifetimes of the mutants were shorter than those of the WT, in agreement with a smaller antenna size (Fig. 2a). A smaller antenna size reduces the distance an excitation has to travel to the RC and increases the probability of the excitation being located on the RC in an energetically equilibrated system. On the other hand, functionally disconnected antenna, closed PSII and free Chls all have long fluorescence lifetimes (>1 ns), and the long-lived component present in all the mutants has a very small amplitude (≤4 %; Supplementary Table 1). Importantly, this indicates that the minor antenna complexes present in koLHCII are functionally connected to the PSII core.

Due to the difficulty in achieving a fully closed state in isolated membranes, these measurements were performed on leaves infiltrated with 3-(3,4-dichlorophenyl)-1,1-dimethylurea (DCMU), which blocks forward electron transport beyond Q_A^-. PSII was successfully closed with the excitation beam and measurements were performed under annihilation-free conditions (Supplementary Fig. 2). The antenna mutants display significantly shorter fluorescence lifetimes than WT (Fig. 2b). This static quenching lowers both steady-state F_v/F_m and NPQ values in the antenna mutants, highlighting the need to use time-resolved fluorescence data to calculate the rate of NPQ, which is independent of closed-state lifetime.

Intrinsic rate of NPQ

The overall quenching lifetime of NPQ τ_{NPQ} is the inverse of the rate of NPQ k_{NPQ} and can be determined using the acquired steady-state and time-resolved data with the equation

$$\tau_{NPQ} = \frac{\tau_m}{NPQ} \quad (1)$$

(see Supplementary Note 1 for details on how this equation is derived). The meaning of τ_{NPQ} can be easily understood by making a parallel with the trapping of excitations in the RC of PSII. It is well-known (see ref. 39) that the corresponding lifetime τ_{trap} of that process can be written as

$$\tau_{trap} = \tau_{CS} + \tau_{mig} \quad (2)$$

where the migration time τ_{mig} is the average time it takes for an excitation to reach the primary electron donor in the RC for the first time. It can also be considered as an excitation equilibration time. The overall charge separation time τ_{CS}, on the other hand, denotes the charge separation after equilibration. This time is equal to the intrinsic charge separation time τ_{ics} (when the excitation is on the primary electron donor), divided by the probability p_{pd} that the primary donor *pd* is in the excited state according to the Boltzmann distribution

$$p_{pd} = \frac{e^{-\frac{E_{pd}}{kT}}}{\sum_i e^{-\frac{E_i}{kT}}}. \quad (3)$$

Here the summation runs over all pigments i with excited state E_i in the photosystem and includes the primary donor *pd* with excited-state energy E_{pd}. The Boltzmann constant and absolute temperature are denoted with k and T, respectively. This then leads to

$$\tau_{trap} = \frac{\tau_{ics}}{p_{pd}} + \tau_{mig}. \quad (4)$$

In case all N Chls *a* are isoenergetic

$$p_{pd} = \frac{1}{N} \quad (5)$$

https://doi.org/10.1038/s41467-026-74992-z

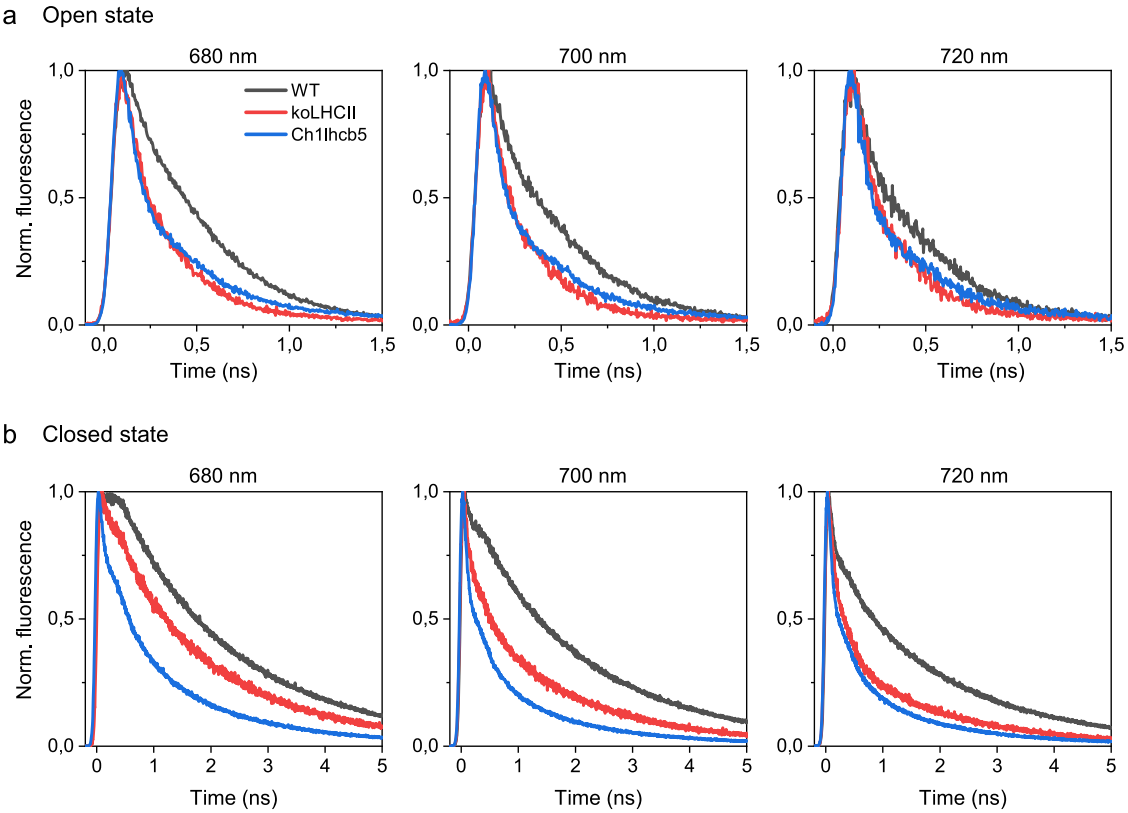

Fig. 2 | Normalized fluorescence decay curves of WT and antenna mutants. **a** Time-resolved fluorescence measurements performed on thylakoid membranes in the open state. Traces are representative of more than 3 biologically independent replicas with similar results. **b** Time-resolved fluorescence measurements performed on leaves in the closed state. The closed state is obtained via leaf infiltration with 200 µM DCMU. Traces are representative of 7, 6, and 5 biologically independent replicas with similar results for WT, koLHCII and Ch1lhcb5, respectively. Samples were excited at 468 nm and fluorescence was detected at 680, 700 and 720 nm.

and

$$\tau_{trap} = N\tau_{ics} + \tau_{mig}. \quad (6)$$

Exactly the same formalism can be used to describe quenching due to NPQ instead of quenching due to trapping in the RC:

$$\tau_{NPQ} = \frac{\tau_{NPQ'}}{p_{npq}} + \tau'_{mig} \quad (7)$$

Here τ_{NPQ}' is the inverse of the intrinsic rate of NPQ when the excitation is at the quenching site, τ_{mig}' is the average time taken for an excitation to reach the quenching site, and p_{npq} is the probability that the excitation is on the quenching site, i.e. on the Chl that is directly being quenched. In line with the Boltzmann distribution, p_{npq} can be approximated by $1/N$, where N is the number of isoenergetic Chl *a* molecules per supercomplex (Supplementary Table 2). If there is more than one quencher per supercomplex, then the corresponding rates can simply be summed, leading to a combined overall rate of quenching. Given that both τ_{mig}' and p_{npq} depend on antenna size, it is necessary to calculate τ_{NPQ}' for a quantitative comparison of NPQ capacity between WT and the antenna mutants.

Like trapping in the RC, the nature of the quenching process lies somewhere in between a trap-limited case where τ_{mig}' is infinitely short and a migration-limited case where τ_{CS} is infinitely short. In the fully trap-limited case, τ_{NPQ}' can be calculated as:

$$\tau_{NPQ'} = \frac{\tau_{NPQ}}{N} \quad (8)$$

In the migration-limited scenario, the exact value of τ_{NPQ} may depend slightly on the location of the quenching site (see ref. 40), but here we assume that τ_{mig}' is equal to τ_o, which is correct if trapping in the RC is fully migration-limited and there is one quencher per RC. τ_o is the average migration time from anywhere in the photosystem to the RC. In the case the number of quenchers is one or more per photosystem, this should be considered an absolute upper limit for τ_{mig}' because energy transfer from the core antenna (CP43 and CP47) to the RC is relatively slow and the time to reach a quenching site would be somewhat shorter. On the other hand, if the number of quenchers would be somewhat smaller than the number of RCs, then the migration time would be somewhat longer. However, because the overall trapping time is known to be at least partly trap-limited, we use τ_o as a reasonable value for the migration time. Therefore, in the migration-limited scenario τ_{NPQ}' can be calculated as:

$$\tau_{NPQ'} = \frac{\tau_{NPQ} - \tau_o}{N} \quad (9)$$

In the trap-limited scenario, WT, koLHCII and Ch1lhcb5 have intrinsic rates of quenching k_{NPQ}' of $(4\,\text{ps})^{-1}$, $(14\,\text{ps})^{-1}$, and $(24\,\text{ps})^{-1}$, while in the migration-limited scenario they have intrinsic rates of quenching k_{NPQ}' of $(3\,\text{ps})^{-1}$, $(13\,\text{ps})^{-1}$ and $(20\,\text{ps})^{-1}$. These rates are expressed relative to the rate in WT in Fig. 3a. Assuming that the quenching in the various PSII compartments occurs in a similar mechanistic way between WT and mutants, it is possible to calculate

https://doi.org/10.1038/s41467-026-74992-z

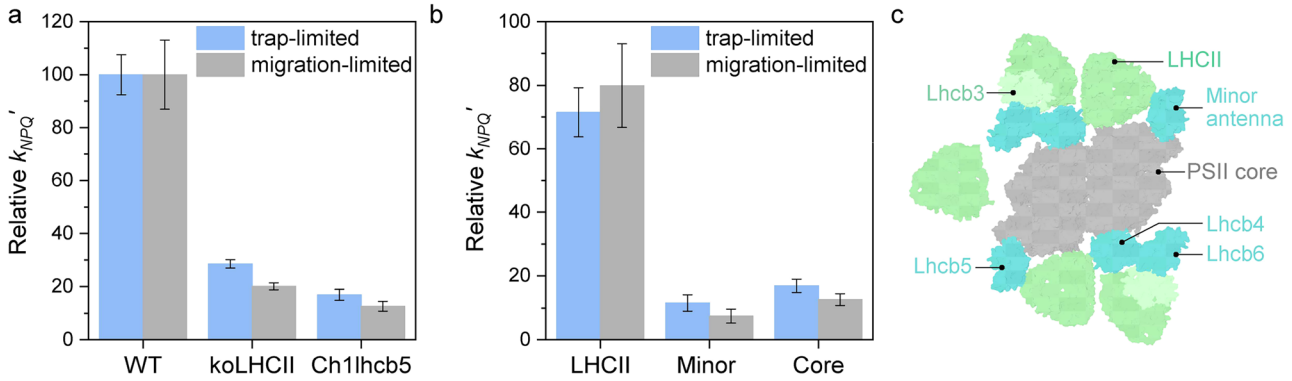

Fig. 3 | Intrinsic rates of NPQ (k_{NPQ}') in both trap- and migration-limited scenarios. a The k_{NPQ}' of each antenna mutant relative to WT. Error bars represent propagated standard errors from at least three biological replicas. **b** The proportion of k_{NPQ}' occurring in each PSII compartment in WT. Error bars represent propagated standard errors from at least three biological replicas. **c** Model of the dimeric PSII supercomplex, including an additional loosely bound trimer to represent the 2.5 LHCII trimers present per PSII core monomer in WT under normal growth conditions. PDB code: 5XNL (*15*).

the k_{NPQ}' for each PSII compartment according to:

$$k_{NPQ}'(core) = k_{NPQ}'(Ch1lhcb5) \quad (10)$$

$$k_{NPQ}'(minor) = k_{NPQ}'(koLHCII) - k_{NPQ}'(Ch1lhcb5) \quad (11)$$

$$k_{NPQ}'(LHCII) = k_{NPQ}'(WT) - k_{NPQ}'(koLHCII) \quad (12)$$

The contribution of each compartment to NPQ can then be expressed as a proportion of the total k_{NPQ}' occurring in WT. For example:

$$Core = \frac{k_{NPQ}'(core)}{k_{NPQ}'(WT)} \times 100 \quad (13)$$

In both trap- and migration-limited scenarios, this results in LHCII being responsible for 70-80% of quenching in WT, the minor antenna for 6-12% and the core for 13-17% (Fig. 3b).

Above we made the assumption that all Chl *a* molecules are isoenergetic, mainly for presenting a simplified calculation, but this assumption influences the calculated quenching efficiency of the quencher by no more than 1% (see also SI).

At wavelengths above 700 nm PSI contributes substantially to fluorescence emission, and so far, this contribution has been ignored. If the results are corrected for each plant's individual PSI contribution, the absolute rates decrease; however, the relative rates remain much the same (Supplementary Note 2; Supplementary Table 3, 4; and Supplementary Fig. 3), reflecting that the conclusions are not affected by PSI.

Discussion

Determining the location of NPQ in the PSII supercomplex is not trivial. Reverse genetic approaches, removing different combinations of pigment-protein complexes, can often have unintended secondary consequences, i.e. upregulation of other pigment-protein complexes or poor connection of the remaining complexes to the PSII core[41,42], making it difficult to accurately quantify the proportion of NPQ occurring in each compartment.

Previous studies have shown that the level of NPQ decreases substantially in the absence of the antenna complexes. In particular, a mutant of *Arabidopsis* lacking Lhcb1 and Lhcb2 (NoL), and the Chl *b*-deficient mutant (Ch1) in which almost all peripheral antenna complexes fail to accumulate, both displayed a ~60% reduction in NPQ[33]. These observations suggested that the majority of quenching occurs in LHCII, a significant fraction occurs in the PSII core, and only a minor contribution arises from the minor antenna complexes. In the present study, we measured NPQ in the koLHCII mutant, which lacks all LHCII subunits, including Lhcb3, in contrast to the NoL mutant where Lhcb3 was still present. However, NPQ levels in the koLHCII and NoL mutant are almost identical, indicating that Lhcb3 plays only a minor role in NPQ.

We also analyzed the Ch1Lhcb5 mutant, which, in addition to the Ch1 background, lacks the Lhcb5 apoprotein, the only remaining minor antenna component in Ch1[30].

To get quantitative information about the partitioning of NPQ, we have performed time-resolved fluorescence measurements on WT and the antenna mutants. In the open state, each sample displays a lifetime proportional to its antenna size, as has previously been observed in WT plants acclimated to different light conditions and in isolated PSII supercomplexes[21,43]. This result indicates that the remaining antenna complexes are well connected to the core and that there are no major alterations in the functional connectivity between complexes with respect to the WT. The near absence of long-lived fluorescence (>1 ns) in all antenna mutants in the open state supports the good functional connectivity of the remaining complexes. In koLHCII, this demonstrates that LHCII is not required for the functional connection of the minor antennae to the core, which is reasonable given that LHCII is the outermost antenna of the supercomplex.

Surprisingly, in the closed state, each plant displays a lifetime proportional to physical antenna size. The reduction of F_v/F_m and, at least part of the reduction of NPQ in the antenna mutants can therefore be attributed to a reduction in F_m due to static quenching (i.e. quenching in the absence of ΔpH). The correlation of closed-state lifetime to physical antenna size suggests that LHCs stabilize the PSII core in a light-harvesting conformation, perhaps by controlling the macro-organization of complexes and preventing the clustering of PSII cores. It is also possible that the closed PSII reaction center is acting as a weak quencher. The quencher would become more populated in the absence of LHCs resulting in a shorter lifetime. It is worth noting that cyanobacterial PSII, which lacks integral membrane LHCs, also has a relatively short lifetime in the closed state in vivo[44,45].

Using both steady-state and time-resolved fluorescence data, it was possible to calculate the *intrinsic* rate of NPQ (k_{NPQ}') for each plant. The differences in k_{NPQ}' between WT, koLHCII and Ch1lhcb5 provide us with the k_{NPQ}' of each PSII compartment, and from this, it is estimated that in WT plants ~70-80% of quenching occurs in LHCII, less than 10% occurs in the minor antennae (and Lhcb3), and 15-20% occurs in the

PSII core. This result was obtained assuming 2.5 LHCII trimers per PSII reaction center, estimated from the measured Chl a/b ratio and the PSI/PSII ratio, as described previously[46]. Importantly, varying this value between 2 and 3 LHCII trimers per PSII-RC had only a minimal effect on the partitioning (see Supplementary Table 5), well within the calculated error range. If k_{NPQ}' is normalized to the number of Chls *a* in each compartment to account for their differences in size, this results in LHCII being at least twice as efficient at quenching as either the minor antenna or the core. Note that the trap-limited model leads to the lowest value for the contribution of LHCII to the quenching, which is 70%. In the migration-limited case, the contribution of LHCII is larger, and it might even exceed 80% in the case there is less than one quencher for Photosystem II RC. For example, if the migration time to the quencher is 50% slower than that to the reaction center, the contribution of LHCII increases by less than 5%. More accurate quantitative estimates will be possible using the approach proposed here once the number of quenchers per PSII reaction center and the migration time to the quenchers are better constrained.

It has previously been reported that the rate of NPQ (or alternatively the number of quenchers) is higher in the presence of closed RCs than in the presence of open RCs[45], which is in accordance with the presence of multiple quenching sites in the present study. The current NPQ experiments were performed in the presence of closed RCs and do not allow us to determine which quenching sites remain active for open RCs.

It should be emphasized that this model assumes that the loss of LHCII trimers in koLHCII or the loss of Lhcb complexes in Ch1lhcb5 does not affect the quenching properties of the remaining antenna or the core. This also implies that the quenching at all sites is independent of each other, as has been previously suggested[23,24]. Moreover, our results indicate that in all mutants, the remaining complexes are well connected.

In summary, the current study highlights the limitations of using steady-state fluorescence alone to assess the capacity of antenna mutants to perform NPQ. We show that relatively simple time-resolved measurements can be utilized to gain insight into the energetic connectivity of the PSII supercomplex, identify the presence of static quenching, and estimate intrinsic rates of quenching. Our results demonstrate that NPQ does in fact occur in each compartment of the PSII supercomplex, providing support for previously proposed multisite models of quenching.

Methods

Arabidopsis growth conditions and thylakoid isolation

Arabidopsis thaliana WT (Col-0), koLHCII[36] and Ch1lhcb5[47] were grown under 120 µmol photons m^{-2} s^{1}, 21 °C/18 °C, for 4–8 weeks. 3 replicas of two independent lines, kolhcII#17 and kolhcII#36, were used for the koLHCII mutant. No difference was noted between the two lines. The mutants used in this work have been characterized previously[30,36].

For the thylakoid preparation, Arabidopsis leaves were shortly grinded in a solution containing 20 mM Tricine KOH pH 7.8, 0.4 M sorbitol, 5 mM EDTA-Mn, 5 mM MgCl2 and the protease inhibitors 0.2 mM benzamidine, 1mM h-aminocaproic acid. Solution was filtered through several layers of cheesecloth and centrifuged 10 min at 1400 g. The pellet was resuspended in a solution containing 20 mM Tricine KOH pH 7.8, 150 mM sorbitol, 5 mM MgCl2, 2.5 mM EDTA-Mn, and the protease inhibitors 0.2 mM benzamidine, 1 mM h-aminocaproic acid. This solution was centrifuged 10 min at 4000 g, pellet was resuspended in a solution containing 5 mM MgCl2, 15 mM NaCl, and 20 mM Hepes KOH pH 7.5, and centrifuged again 10 min at 6000 g. Pellet was finally resuspended in a small volume of the last solution. The entire preparation was done in a cold room. Thylakoids underwent one freeze-thaw cycle (flash frozen in liquid nitrogen, stored at -80 °C and thawed on ice) with no effect on results.

Pigment and protein analysis

Pigments were extracted from thylakoid membranes with 80% acetone. Room-temperature absorption spectra of the pigment extracts were recorded on a Varian Cary 4000 UV–vis spectrophotometer. Chl *a*/*b* and Chl/Car ratios were calculated by fitting the absorption spectrum of the pigment extract with the spectra of the individual pigments[48].

PAM fluorometry

Using the modular Dual PAM-100 apparatus (Walz), whole leaves were illuminated with a measuring light (460 nm, 3 µmol photons m^{-2} s^{-1}), and chlorophyll fluorescence emission was detected at wavelengths above 700 nm. The minimum level of fluorescence (F_o) was measured after 1 h of dark adaptation. The maximum level of fluorescence (F_m) was detected by applying a saturating pulse (635 nm, 180 ms, 12,000 µmol photons m^{-2} s^{-1}) to dark-adapted leaves. Leaves were then light-adapted for 8 min with an actinic light sufficient to saturate NPQ in all plants (635 nm, 1,200 µmol photons m^{-2} s^{-1})[33]. This was followed by 10 min of recovery in darkness. The maximal level of fluorescence of the light-adapted sample (F_m') was detected every 20 s with a saturating pulse. F_v/F_m was calculated as $(F_m - F_o) \cdot F_m^{-1}$. NPQ was calculated as $(F_m - F_m') \cdot F_m'^{-1}$ and reported as the difference in the maximum level of NPQ in light and the minimum level of NPQ following dark recovery.

Time-correlated single-photon counting (TCSPC)

Time-resolved fluorescence measurements were performed with a FluoTime 200 fluorometer (PicoQuant). Excitation was provided by a 468 nm laser diode, and fluorescence emission was detected sequentially at 680, 700 and 720 nm. Thylakoid samples were diluted to an OD of 0.05 cm^{-1} at the Q_y maximum and a volume of 3 mL in 15 mM NaCl, 15 mM $MgCl_2$ and 10 mM Hepes/KOH pH 7.5. The sample was kept at 20 °C and stirred in a cuvette with a path length of 1 cm. The laser repetition rate was set to 10 MHz, and the power was reduced to 0.5–3 µW using neutral density filters (Supplementary Fig. 2). Each measurement had a maximum acquisition time of 15 min. A measurement with 680 nm detection was repeated at the end of each measuring sequence to ensure RCs remained open throughout the measurement.

Whole leaves were taken from dark-adapted plants and incubated in a 0.3 M sorbitol, 10 mM Hepes pH 7.5, 200 µM DCMU solution for 4 h. Successful DCMU infiltration was confirmed by ensuring that there was no difference in F_m under low actinic light illumination (i.e. 50 µmol photons m^{-2} s^{-1}) and a saturating pulse (3000 µmol photons m^{-2} s^{-1}) in the Dual PAM. The leaf was inserted at an approximately 45-degree angle relative to both the excitation beam and the detector. Scattered light was blocked with an optical long-pass filter prior to detection. Laser repetition rate was set to 2.5 MHz and the power kept between 1–20 µW (Supplementary Fig. 3) to sufficiently close the PSII reaction centers while also avoiding singlet-singlet annihilation. A measurement with 680 nm detection was repeated at the end of each measuring sequence to ensure there was no photoinhibitory quenching occurring throughout the measurement.

Fluorescence decay curves were analyzed using FluoFit software (PicoQuant), following deconvolution of the instrument response function (IRF; 88 ps full width at half maximum) measured from the ~6 ps decay of pinacyanol iodide-dye dissolved in methanol[49] or with scattering powder. Examples of the fittings are shown in Supplementary Figs. 4 and 5. The data were globally fitted to multi-exponential decay functions with amplitudes A_i and associated fluorescence decay times τ_i. The average fluorescence lifetimes were calculated according to $\tau_{avg} = \Sigma A_i * \tau_i / \Sigma A_i$.

Reporting summary

Further information on research design is available in the Nature Portfolio Reporting Summary linked to this article.

Data availability

Source data are provided with this paper.

References

1. Croce, R. & van Amerongen, H. Light harvesting in oxgenic photosynthesis: structural biology meets spectroscopy. *Science* **369**, eaay2058 (2020).
2. Belgio, E., Johnson, M. P., Juric, S. & Ruban, A. V. Higher plant photosystem II light-harvesting antenna, not the reaction center, determines the excited-state lifetime-both the maximum and the nonphotochemically quenched. *Biophys. J.* **102**, 2761–2771 (2012).
3. Gilmore, A. M. & Hazlett, T. L. & Govindjee. Xanthophyll cycle-dependent quenching of photosystem II chlorophyll a fluorescence: formation of a quenching complex with a short fluorescence lifetime. *Proc. Natl. Acad. Sci. USA.* **92**, 2273–2277 (1995).
4. Aro, E. M., Virgin, I. & Andersson, B. Photoinhibition of photosystem-2 - inactivation, protein damage and turnover. *Biochim. Biophys. Acta* **1143**, 113–134 (1993).
5. Krieger-Liszkay, A., Fufezan, C. & Trebst, A. Singlet oxygen production in photosystem II and related protection mechanism. *Photosynth. Res.* **98**, 551–564 (2008).
6. van Amerongen, H. & Croce, R. Nonphotochemical quenching in plants: mechanisms and mysteries. *Plant Cell*. **37**, koaf240 (2025).
7. Marulanda Valencia, W. & Pandit, A. Photosystem II subunit S (PsbS): a nano regulator of plant photosynthesis. *J. Mol. Biol.* **436**, 168407 (2024).
8. Bassi, R. & Dall'Osto, L. Dissipation of light energy absorbed in excess: the molecular mechanisms. *Annu Rev. Plant Biol.* **72**, 47–76 (2021).
9. Ruban, A. V. & Wilson, S. The mechanism of non-photochemical quenching in plants: localization and driving forces. *Plant Cell Physiol.* **62**, 1063–1072 (2021).
10. Briantais, J. M., Vernotte, C., Picaud, M. & Krause, G. H. A quantitative study of the slow decline of chlorophyll a fluorescence in isolated chloroplasts. *Biochim. Biophys. Acta* **548**, 128–138 (1979).
11. Li, X. P. et al. A pigment-binding protein essential for regulation of photosynthetic light harvesting. *Nature* **403**, 391–395 (2000).
12. Li, X. P. et al. Regulation of photosynthetic light harvesting involves intrathylakoid lumen pH sensing by the PsbS protein. *J. Biol. Chem.* **279**, 22866–22874 (2004).
13. Niyogi, K. K., Grossman, A. R. & Björkman, O. Arabidopsis mutants define a central role for the xanthophyll cycle in the regulation of photosynthetic energy conversion. *Plant Cell* **10**, 1121–1134 (1998).
14. Jahns, P. & Holzwarth, A. R. The role of the xanthophyll cycle and of lutein in photoprotection of photosystem II. *Biochim. Biophys. Acta* **1817**, 182–193 (2012).
15. Ruban, A. V. Nonphotochemical chlorophyll fluorescence quenching: mechanism and effectiveness in protecting plants from photodamage. *Plant Physiol.* **170**, 1903–1916 (2016).
16. Wei, X. et al. Structure of spinach photosystem II-LHCII supercomplex at 3.2 A resolution. *Nature* **534**, 69–74 (2016).
17. Su, X. et al. Structure and assembly mechanism of plant C2S2M2-type PSII-LHCII supercomplex. *Science* **357**, 815–820 (2017).
18. Dall'Osto, L., Cazzaniga, S., Zappone, D. & Bassi, R. Monomeric light harvesting complexes enhance excitation energy transfer from LHCII to PSII and control their lateral spacing in thylakoids. *Biochim. Biophys. Acta Bioenerg*. 148035, https://doi.org/10.1016/j.bbabio.2019.06.007 (2019).
19. Crepin, A. & Caffarri, S. Functions and evolution of Lhcb isoforms composing LHCII, the major light harvesting complex of photosystem II of green eukaryotic organisms. *Curr. Protein Pept. Sci.* **19**, 699–713 (2018).
20. Kouril, R., Wientjes, E., Bultema, J. B., Croce, R. & Boekema, E. J. High-light vs. low-light: effect of light acclimation on photosystem II composition and organization in Arabidopsis thaliana. *Biochim. Biophys. Acta* **1827**, 411–419 (2013).
21. Wientjes, E., van Amerongen, H. & Croce, R. Quantum yield of charge separation in photosystem II: functional effect of changes in the antenna size upon light acclimation. *J. Phys. Chem. B* **117**, 11200–11208 (2013).
22. Niyogi, K. K. & Truong, T. B. Evolution of flexible non-photochemical quenching mechanisms that regulate light harvesting in oxygenic photosynthesis. *Curr. Opin. Plant Biol.* **16**, 307–314 (2013).
23. Holzwarth, A. R., Miloslavina, Y., Nilkens, M. & Jahns, P. Identification of two quenching sites active in the regulation of photosynthetic light-harvesting. *Chem. Phys. Lett.* **483**, 262–267 (2009).
24. Dall'Osto, L. et al. Two mechanisms for dissipation of excess light in monomeric and trimeric light-harvesting complexes. *Nat. Plants* **3**, 17033 (2017).
25. Ahn, T. K. et al. Architecture of a charge-transfer state regulating light harvesting in a plant antenna protein. *Science* **320**, 794–797 (2008).
26. Mascoli, V. et al. Capturing the quenching mechanism of light-harvesting complexes of plants by zooming in on the ensemble. *Chem* **5**, 2900–2912 (2019).
27. Sardar, S. et al. Molecular mechanisms of light harvesting in the minor antenna CP29 in near-native membrane lipidic environment. *J. Chem. Phys.* **156**, 205101 (2022).
28. Weis, E. & Berry, J. A. Quantum efficiency of photosystem II in relation to energy dependent quenching of chlorophyll fluorescence. *Biochim. Biophys. Acta* **894**, 198–208 (1987).
29. Finazzi, G. et al. A zeaxanthin-independent nonphotochemical quenching mechanism localized in the photosystem II core complex (vol 101, pg 12375, 2004). *Proc. Natl. Acad. Sci. USA.* **101**, 17322–17322 (2004).
30. Havaux, M., Dall'Osto, L. & Bassi, R. Zeaxanthin has enhanced antioxidant capacity with respect to all other xanthophylls in Arabidopsis leaves and functions independent of binding to PSII antennae(1[C][W]). *Plant Physiol.* **145**, 1506–1520 (2007).
31. Townsend, A. J. et al. The causes of altered chlorophyll fluorescence quenching induction in the Arabidopsis mutant lacking all minor antenna complexes. *Biochim. Biophys. Acta Bioenerg.* **1859**, 666–675 (2018).
32. Saccon, F., Giovagnetti, V., Shukla, M. K. & Ruban, A. V. Rapid regulation of photosynthetic light harvesting in the absence of minor antenna and reaction centre complexes. *J. Exp. Bot.* **71**, 3626–3637 (2020).
33. Nicol, L., Nawrocki, W. J. & Croce, R. Disentangling the sites of non-photochemical quenching in vascular plants. *Nat. Plants* **5**, 1177–1183 (2019).
34. Jackowski, G., Kacprzak, K. & Jansson, S. Identification of Lhcb1/Lhcb2/Lhcb3 heterotrimers of the main light- harvesting chlorophyll a/b-protein complex of Photosystem II (LHC II). *Biochim. Biophys. Acta* **1504**, 340–345 (2001).
35. Caffarri, S., Croce, R., Cattivelli, L. & Bassi, R. A look within LHCII: differential analysis of the Lhcb1-3 complexes building the major trimeric antenna complex of higher-plant photosynthesis. *Biochemistry* **43**, 9467–9476 (2004).
36. Guardini, Z. et al. Mapping light-harvesting and photoprotection responses in the Photosystem II antenna system of higher plants. *Plant Physiol.* **199**, https://doi.org/10.1093/plphys/kiaf588 (2025).
37. Baker, N. R. Chlorophyll fluorescence: a probe of photosynthesis in vivo. *Annu. Rev. Plant Biol.* **59**, 89–113 (2008).
38. Chukhutsina, V. U., Liu, X., Xu, P. & Croce, R. The major light-harvesting complex (LHCII) is an antenna of Photosystem I in dark-adapted plants. *Nat. Plants*, https://doi.org/10.1038/s41477-020-0693-4 (2020).

39. Van Amerongen, H., Valkunas, L. & van Grondelle, R. *Photosyntheric excitons*. (World Scientific Publishing Co.Pte.Ldt., 2000).
40. Valkunas, L., Trinkunas, G., Chmeliov, J. & Ruban, A. V. Modeling of exciton quenching in photosystem II. *Phys. Chem. Chem. Phys.* **11**, 7576–7584 (2009).
41. Dall'Osto, L., Unlu, C., Cazzaniga, S. & van Amerongen, H. Disturbed excitation energy transfer in Arabidopsis thaliana mutants lacking minor antenna complexes of photosystem II. *Biochim. Biophys. Acta* **1837**, 1981–1988 (2014).
42. van Oort, B. et al. Effect of antenna-depletion in photosystem II on excitation energy transfer in *Arabidopsis thaliana*. *Biophys. J.* **98**, 922–931 (2010).
43. Caffarri, S., Broess, K., Croce, R. & van Amerongen, H. Excitation energy transfer and trapping in higher plant Photosystem II complexes with different antenna sizes. *Biophys. J.* **100**, 2094–2103 (2011).
44. Tian, L., Farooq, S. & van Amerongen, H. Probing the picosecond kinetics of the photosystem II core complex in vivo. *Phys. Chem. Chem. Phys.* https://doi.org/10.1039/c3cp43813a (2013).
45. Farooq, S. et al. Dynamic feedback of the photosystem II reaction centre on photoprotection in plants. *Nat. Plants* **4**, 225–231 (2018).
46. Unlu, C., Drop, B., Croce, R. & van Amerongen, H. State transitions in *Chlamydomonas reinhardtii* strongly modulate the functional size of photosystem II but not of photosystem I. *Proc. Natl. Acad. Sci. USA.* **111**, 3460–3465 (2014).
47. Dall'Osto, L., Caffarri, S. & Bassi, R. A mechanism of non-photochemical energy dissipation, independent from PsbS, revealed by a conformational change in the antenna protein CP26. *Plant Cell* **17**, 1217–1232 (2005).
48. Croce, R., Canino, G., Ros, F. & Bassi, R. Chromophore organization in the higher-plant photosystem II antenna protein CP26. *Biochemistry* **41**, 7334–7343 (2002).
49. van Oort, B. et al. Picosecond fluorescence of intact and dissolved PSI-LHCI crystals. *Biophys. J.* **95**, 5851–5861 (2008).

Acknowledgements

We thank Eduard Elias (VU Amsterdam) for his help in setting up the experiments.

Author contributions

R.C. and H.v.A. devised the project. L.N., A.C., H.Y and V.M. performed experiments. L.D'O. and R.B. provided the koLHCII mutant. L.N., A.C., H.Y, V.M., H.v.A. and R.C. analyzed and interpreted data. L.N., V.M., H.v.A. and R.C. wrote the manuscript. All authors reviewed and approved the final manuscript.

Funding

Dutch organization for Scientific research Vici grant (RC) and NWO Groot (OCENW.GROOT.2019.086) (RC and HvA), European Union's Horizon 2020 research and innovation program Marie Skłodowska-Curie grant 675006 (RC, HvA). Royal Society of New Zealand Te Apārangi Rutherford Foundation international PhD scholarship (LN) The CSC scholarship (H.Y.).

Competing interests

The authors declare no competing interests.

Additional information

Supplementary information The online version contains supplementary material available at https://doi.org/10.1038/s41467-026-74992-z.

Correspondence and requests for materials should be addressed to Roberta Croce.

Peer review information *Nature Communications* thanks Tomas Polivka, and the other, anonymous, reviewer(s) for their contribution to the peer review of this work. A peer review file is available.